Check for updates

Analysis, circuit realization and controls of an autonomous Morse jerk oscillator

Cyrille Ainamon[1] · Victor Kamdoum Tamba[2,3] · Justin Roger Mboupda Pone[3] ·
Sifeu Takougang Kingni[4] · Hubert Boudoue Malwe[5] · Jean Bio Chabi Orou[1]

Abstract

In this paper, an autonomous Morse jerk oscillator which is designed by converting an autonomous two-dimensional Morse oscillator to a jerk oscillator, is analysed. The stability of its unique equilibrium point reveals the existence of Hopf bifurcation. Periodic and chaotic oscillations, antimonotonicity, chaotic bubbles and coexisting attractors are generated in the proposed jerk oscillator. Then, this proposed jerk oscillator is implemented in PSIM software and realized in a printed circuit board to verify the numerical results. The experimental/PSIM results agree well with the numerical simulations. Moreover, it is possible to control partially or totally the amplitude of its signals by introducing two additional parameters in the rate-equations describing the proposed jerk oscillator. Furthermore based on the Routh–Hurwitz conditions and using a single linear feedback controller, the proposed jerk oscillator is controlled to its unique equilibrium point. Finally, the coexistence between periodic and chaotic attractors is destroyed and controlled to a desired trajectory thank to the linear augmentation method.

✉ Sifeu Takougang Kingni
  stkingni@yahoo.fr

[1] Institut de Mathématiques et de Sciences Physiques, Université d'Abomey-Calavi, B.P. 613, Porto Novo, Benin

[2] Department of Telecommunication and Network Engineering, IUT-Fotso Victor of Bandjoun, University of Dschang, PO Box 134, Bandjoun, Cameroon

[3] Electrical Engineering Department of IUT-Fotso Victor of Bandjoun, Research Unit of Automation and Applied Computer (RU-AIA), University of Dschang, PO Box 134, Bandjoun, Cameroon

[4] Department of Mechanical, Petroleum and Gas Engineering, Faculty of Mines and Petroleum Industries, University of Maroua, PO Box 46, Maroua, Cameroon

[5] Department of Physics, Faculty of Science, University of Maroua, PO Box 814, Maroua, Cameroon

1 Introduction

Chaotic behaviors have been found in many different systems, such as weather and climate [39], economical [19], mechanical [4], biological [14], electronics systems [13], optoelectronics systems [12], optical systems [22] and optomechanics systems [5]. Chaos has been found useful with great potential in many fields, including liquid mixing with low power consumption, human brain and heartbeat regulation and secure communications [3, 18, 32, 33, 45]. One of the important research directions is constructing robust chaotic oscillators with simple structures [31, 35, 42, 43]. There are two kinds of chaotic oscillators: Non-autonomous [44] and autonomous oscillators [37]. Among the existing autonomous chaotic oscillators, there is a family of chaotic oscillators with easy electronic implementation described by a three-dimensional differential equation of the form $\dddot{x} = f(x, \dot{x}, \ddot{x})$. It is called a jerk equation where x, $\dot{x}$, $\ddot{x}$ and $\dddot{x}$ represent a dynamical variable, first-, second-, third-order time derivative, respectively [42]. Autonomous chaotic jerk oscillators attracted increasingly much attention due to their simplicity. In [42], Sprott proposed many new jerk oscillators with several nonlinearities that show chaotic behavior with easy electronic implementation. The authors of [9, 17, 50] introduced three autonomous chaotic oscillators using the Van der Pol dynamics immersed into a jerk oscillator. In [30], the authors proposed and studied theoretically and experimentally an autonomous chaotic Duffing oscillator based on a jerk oscillator. By converting the autonomous two-dimensional Van der Pol–Duffing oscillator to a jerk oscillator, the authors of [46] obtained a chaotic Van der Pol–Duffing jerk oscillator and investigated the dynamical behavior of the integer proposed chaotic jerk oscillator, chaos control and synchronization in its fractional-order form. The dynamical analysis, electronic circuit realization and synchronization of a proposed autonomous chaotic Helmholtz jerk oscillator has been studied in [36, 47].

Therefore, this paper proposes an autonomous Morse jerk oscillator which is built by converting the two-dimensional autonomous Morse oscillator into a three-dimensional oscillator using the jerk architecture. Morse oscillator is a two-dimensional equation describing an oscillator with two exponential nonlinearities. It is used as a well-known model for molecular vibrations [23, 27, 34, 49]. Despite the simplicity of the Morse oscillator, its dynamical behavior is extremely rich and research on the area is still going on [1]. The rate-equations describing the proposed jerk oscillator has two exponential nonlinearities and its investigation reveals multistability phenomenon. The multistability feature is usually found in nonlinear dynamics [11, 15, 21]. Multistable oscillators are categorized to oscillators with ordinary multistability [24–26], oscillators with extreme multistability [6–8] and oscillators with megastability [28, 29, 48]. This paper is devoted to the analysis, circuit realization and controls of a proposed autonomous Morse jerk oscillator.

The organization of the paper is as follows: The proposed jerk oscillator is dynamically analysed in the Sect. 2. The circuit realization of the proposed autonomous Morse jerk oscillator is presented in Sect. 3 while Sect. 4 deals with the controls of the signal amplitudes, chaotic behavior and coexisting attractors in proposed jerk oscillator. Finlay, the conclusion is given in Sect. 5.

2 Analytical and numerical analysis of the proposed autonomous Morse jerk oscillator

The autonomous two-dimensional Morse equation is given by [27, 34, 49]:

$$\ddot{x} + \gamma\dot{x} + \beta\left[1 - \exp\left(-\alpha x\right)\right]\exp\left(-\alpha x\right) = 0, \tag{1}$$

where the parameter γ is a dimensionless damping coefficient ($\gamma > 0$), the parameters $\beta\,(\beta > 0)$ and $\alpha\,(\alpha > 0)$ are the dissociation energy and range parameter, respectively. The autonomous Morse Eq. (1) can be converted to a jerk oscillator, as follows:

$$\dot{x} = y, \tag{2a}$$

$$\dot{y} = \delta z, \tag{2b}$$

$$\dot{z} = -z - \gamma y - \beta\left[1 - \exp\left(-\alpha x\right)\right]\exp\left(-\alpha x\right), \tag{2c}$$

where $\dot{x}(t) = y(t)$ and $\ddot{x}(t) = z(t)$. A positive constant parameter δ is added in Eq. (2b) in order to achieve chaotic behavior in system (2) because for $\delta = \alpha = 1$, $\gamma = 0.16$ and by varying the parameter β, the trajectories of system (2) converge to the equilibrium point $O = (0, 0, 0)$ up to $\beta = \gamma = 0.16$ where a Hopf bifurcation occurs followed by period-1-oscillations and periodic spiking oscillations (not shown). By further increasing the value of parameter β, system (2) displays only periodic oscillations. System (2) is dissipative because $\nabla V = \frac{\partial\dot{x}}{\partial x} + \frac{\partial\dot{y}}{\partial y} + \frac{\partial\dot{z}}{\partial z} = -1 < 0$. It has only one equilibrium point $O = (0, 0, 0)$. The characteristic equation of the Jacobian matrix at the equilibrium point $O = (0, 0, 0)$ is:

$$\lambda^3 + \lambda^2 + \gamma\delta\lambda + \alpha\beta\delta = 0. \tag{3}$$

Using the Routh–Hurwitz conditions, this equation has all roots with negative real parts if and only if:

$$\alpha\beta\delta > 0, \tag{4a}$$

$$(\gamma - \alpha\beta)\delta > 0. \tag{4b}$$

Since $\delta > 0$, the equilibrium point $O = (0, 0, 0)$ of system (2) is stable if $\gamma > \alpha\beta$ and unstable for $\gamma < \alpha\beta$. Since the equilibrium point $O = (0, 0, 0)$ changes stability properties, system (2) has either a Hopf bifurcation or transcritical bifurcation at the equilibrium point O for $\beta = \gamma/\alpha$.

Theorem *If $\delta > 0$, then system* (3) *undergoes a Hopf bifurcation at the equilibrium point O when β passes through the critical value $\beta_H = \gamma/\alpha$.*

Proof Let $\lambda = j\omega(\omega > 0$ and $j^2 = -1)$ be a root of Eq. (3). By inserting $\lambda = j\omega$ it into Eq. (3) and separating real and imaginary parts, it is obtained

$$\omega = \omega_0 = \sqrt{\alpha\beta\delta}, \tag{5a}$$

$$\beta_H = \gamma/\alpha. \tag{5b}$$

Differentiating both sides of Eq. (3) with respect to β, it is obtained

$$3\lambda^2 \frac{d\lambda}{d\beta} + 2\lambda \frac{d\lambda}{d\beta} + \gamma\delta \frac{d\lambda}{d\beta} + \alpha\delta = 0 \tag{6a}$$

and

$$\frac{d\lambda}{d\beta} = \frac{-\alpha\delta}{3\lambda^2 + 2\lambda + \gamma\delta} \tag{6b}$$

then

$$\mathrm{Re}\left(\frac{d\lambda}{d\beta}\bigg|_{\beta=\beta_H,\,\lambda=i\omega_0} \right) = -\frac{\alpha}{2\gamma(1+\gamma\delta)} \neq 0. \tag{6c}$$

Since the Jacobian matrix of system (2) at the equilibrium point O has two purely imaginary eigenvalues and the real parts of eigenvalues satisfy $\mathrm{Re}\left(\frac{d\lambda}{d\beta}\big|_{\beta=\beta_H,\,\lambda=i\omega_0} \right) \neq 0$; all the conditions for Hopf bifurcation to occur are met. Consequently, system (2) undergoes a Hopf bifurcation at O when $\beta = \beta_H = \gamma/\alpha$ and periodic solutions will exist in a neighbourhood of the point β_H (provided that $\delta > 0$ holds).

The effect of parameters α, β, γ and δ on the dynamics behaviours of system (2) can be studied by using numerical simulations. So, to identify the dynamical behaviours of system (2), the two parameters largest Lyapunov exponents (LLE) diagrams are constructed in Fig. 1.

From Fig. 1a, it is clear that colors are associated with the magnitude of the LLE as follows: blue stands for the negative LLE and positive LLE is indicated by a continuously changing between light blue–red scale passing through green and yellow scales. On LLE diagram in (δ, β) space, chaotic regions are characterized as a combination of light blue–green–yellow–red colors and periodic regions are characterized by blue colors. In Fig. 1b, chaotic regions are illustrated as a combination of light blue–green–yellow–red colors and periodic regions are illustrated by blue and light blues on LLE diagram in (γ, β) space. In order to know the route to chaotic behavior
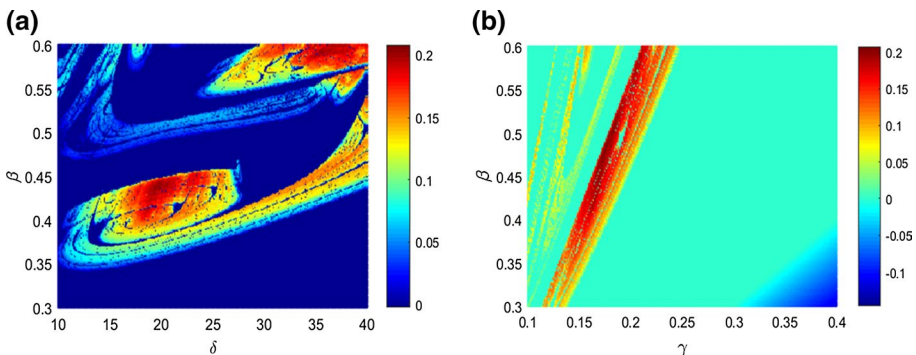

Fig. 1 (Colour online) Two parameters LLE diagrams in: **a** (δ, β) space for $\gamma = 0.16$ and **b** (γ, β) space for $\delta = 18$. The other parameter is $\alpha = 1$
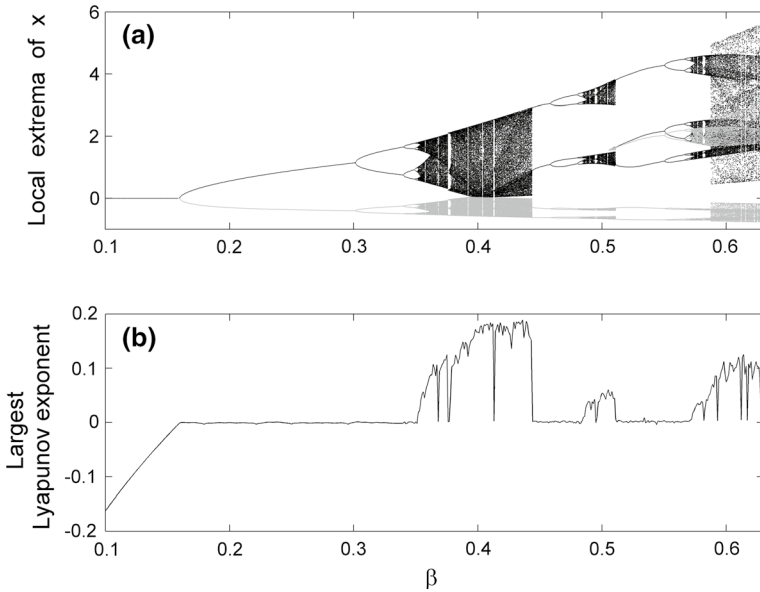
Fig. 2 The bifurcation diagram depicting the local maxima (black dots) and local minima (gray dots) of $x(t)$ (**a**) and the LLE (**b**) versus the parameter β for $\alpha = 1$, $\gamma = 0.16$ and $\delta = 18$

exhibited by system (2), the bifurcation diagrams depicting the local extrema of $x(t)$ as a function of the parameter β or δ for specific values of δ or β are plotted.

In Fig. 2a, the trajectories of system (2) converge to the equilibrium point $O = (0, 0, 0)$ up to $\beta = \gamma / \alpha \approx 0.16$, where a Hopf bifurcation occurs followed by period-1-oscillations and period-doubling to chaos interspersed with periodic windows. Therefore, the above analytical calculations about Hopf bifurcation are confirmed by Fig. 2a. The LLE of Fig. 2b confirms the dynamical behaviors found in Fig. 2a. The phase portraits of chaotic oscillations for specific values of the parameter β are plotted in Fig. 3.

System (2) displays one scroll-chaotic attractor as shown in Fig. 3. For $\alpha = 1$, $\gamma = 0.16$ and $\beta = 0.4$, the bifurcation diagram of $x(t)$ and the corresponding LLE versus the parameter δ is presented in Fig. 4.
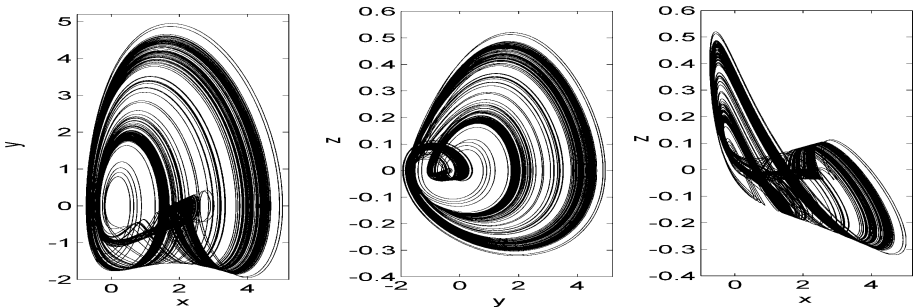

Fig. 3 The phase portrait of system (2) in planes (x, y), (y, z) and (x, z) with $\beta = 0.6$, $\alpha = 1$, $\gamma = 0.16$ and $\delta = 18$. Initial conditions $(x(0), y(0), z(0)) = (0.1, 0.1, 0.1)$
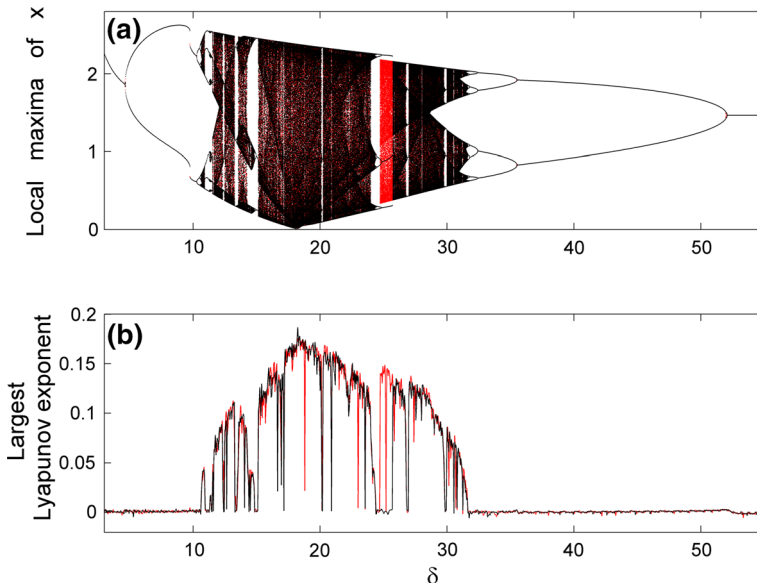
Fig. 4 (Colour online) Bifurcation diagram depicting the maxima of $x(t)$ (**a**) and the corresponding LLE (**b**) versus the parameter δ for $\alpha = 1$, $\gamma = 0.16$ and $\beta = 0.4$. Bifurcation diagrams are obtained by scanning the parameter δ upwards (black) and downwards (red)

In Fig. 4a, these forward and reverse period doubling sequences when a parameter δ increases (or decreases) in a monotone way, called antimonotonicity [10, 16] is revealed. By comparing the two set of data [for increasing (black) and decreasing (red)] used to plot Fig. 4a, Fig. 4a displays coexistence of attractors between period-6-oscillations and chaotic oscillations for $24.74 \leq \delta \leq 24.88$ and coexistence of attractors between period-3-oscillations and chaotic oscillations in the range $24.88 < \delta \leq 25.74$. The dynamical behavior found in Fig. 4a are confirmed by the LLE shown in Fig. 4b.

The bifurcation diagrams depicting the maxima of $x(t)$ versus the parameter δ are computed for some specific values of parameter β as depicted in Fig. 5 in order to illustrate the mechanism of the antimonotonicity phenomenon found in Fig. 4.

Chaotic oscillations and bubbles [10] are presented in Fig. 5a, b, respectively while only periodic bubbles are found in Fig. 5c–f. For a specific value of parameters β and δ, the phase portraits of the chaotic bubble presented in Fig. 5b and the first-return map of the local maxima of $x(t)$ are plotted in Fig. 6.

The chaotic bubble attractor presented in Fig. 6a–c is confirmed by the numerical calculation of the Lyapunov exponents which gives $LE_1 \approx 0.0412624$, $LE_2 \approx 0$ and $LE_3 \approx -1.03952$. The Kaplan–Yorke dimension of the chaotic bubble is $D_{KY} \approx 2.0396937$. In Fig. 6d, the map is indicative of one-dimensional maps with two critical points p_1 and p_2, which support the occurrence of antimonotonicity phenomenon in the proposed jerk oscillator according to the results of Dawson et al. [16].

The coexistence of attractors found in Fig. 4 is further detailed in Figs. 7, 8.

At $\delta = 24.8$, the output $x(t)$ displays period-6-oscillations and one scroll-chaotic attractor for two different initial conditions as shown in Figs. 7a1, a2, respectively. Period-3-oscillations and one scroll-chaotic attractor are revealed in Fig. 7b1, b2, respectively at $\delta = 25$ for two different initial conditions. The coexistence of attractors
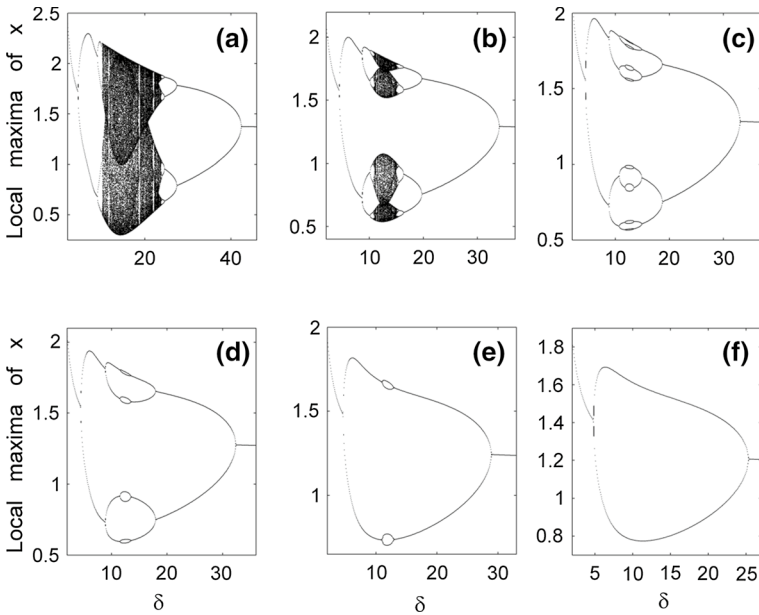
Fig. 5 Bifurcation diagrams depicting the maxima of $x(t)$ versus parameter δ for specific values of parameter β: **a** The chaotic oscillations at $\beta = 0.37$, **b** chaotic bubble at $\beta = 0.345$, **c** bubble of period 16 at $\beta = 0.342$, **d** bubble of period 8 at $\beta = 0.34$, **e** bubble of period 4 at $\beta = 0.33$ and **f** bubble of period 2 at $\beta = 0.32$. The others parameters are given in Fig. 4
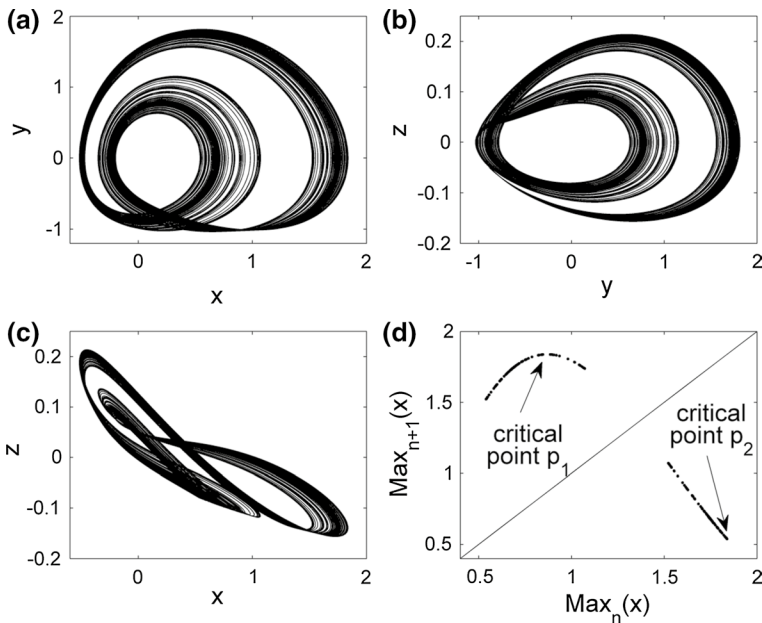

Fig. 6 Phase portraits in plane (x, y) (**a**), (y, z) (**b**), (x, z) (**c**) and the first-return map $(\text{Max}_{n+1}(x) = f(\text{Max}_n(x)))$ of the maxima of $x(t)$ (**d**) for $\alpha = 1, \gamma = 0.16, \beta = 0.345$ and $\delta = 12.85$ with the initial conditions $(x(0), y(0), z(0)) = (0.1, 0.1, 0.1)$
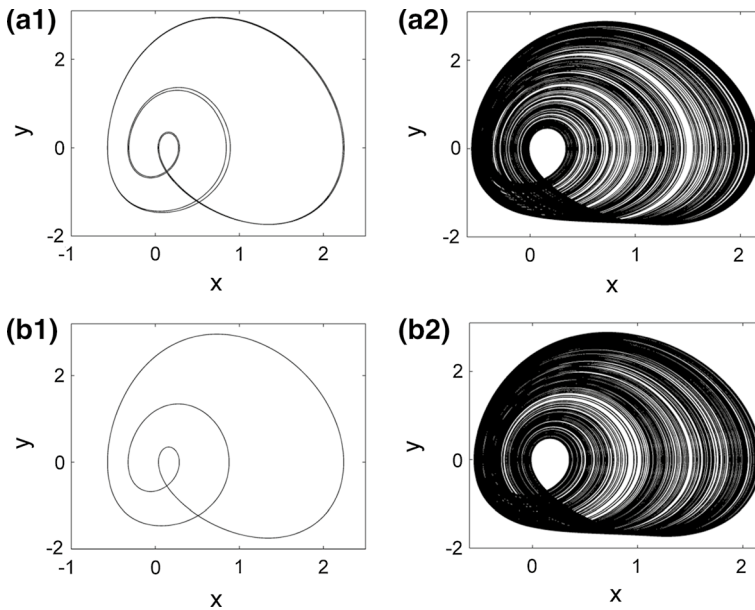
Fig. 7 Coexistence of attractors for specific values of δ and initial conditions: **a1** $\delta = 24.8$ and $(x(0), y(0), z(0)) =(0.0545, 0.1829, 0.0358)$, **a2** $\delta = 24.8$ and $(x(0), y(0), z(0)) = (0.1, 0.1, 0.1)$, **b1** $\delta = 25$ and $(x(0), y(0), z(0)) = (0.0545, 0.1829, 0.0358)$, **b2** $\delta = 25$ and $(x(0), y(0), z(0)) = (0.1, 0.1, 0.1)$. The remaining parameters are given in Fig. 4

Fig. 8 (Color online) Cross section of the basin of attraction of system (2) in the (x, y) plane at z=0. Periodic attractors are in green colour and chaotic attractors are in black colour. The parameters values are $\delta = 25$,$\alpha = 1$,$\gamma = 0.16$ and $\beta = 0.4$
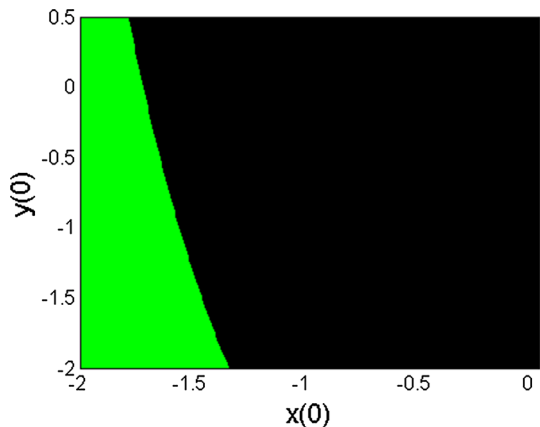
found in Fig. 7 is illustrated in Fig. 8 which depicts the cross section of the basin of attraction of system (2) for specific value of parameter δ.

The black and green regions in Fig. 8 contain initial conditions that lead to the chaotic and periodic behaviors, respectively. The basin of attraction of Fig. 8 shows the possibility of occurrence of chaotic attractors is greater than the one of periodic attractors. The periodic region is located in the range $-2 \leq x(0) < -1.35$ while the chaotic region is found in the range $-1.35 < x(0) \leq 0$.

3 Electronic realization of the proposed autonomous Morse jerk oscillator

The aim of this section is to realize the electronic circuit describing the proposed jerk oscillator and point out some experimental/PSIM results in order to validate the numerical simulation results of Sect. 2. The circuit of the proposed autonomous Morse jerk oscillator is designed and realized in Fig. 9.

Figure 9 consists of resistors, capacitors, operational amplifiers, analogue multiplier device M (AD633JN integrated circuit) and diode D (1N4148). The current flowing inside
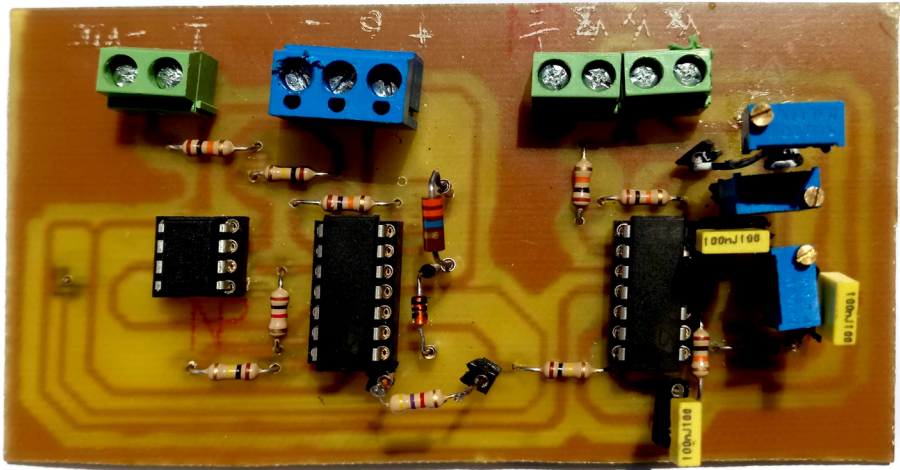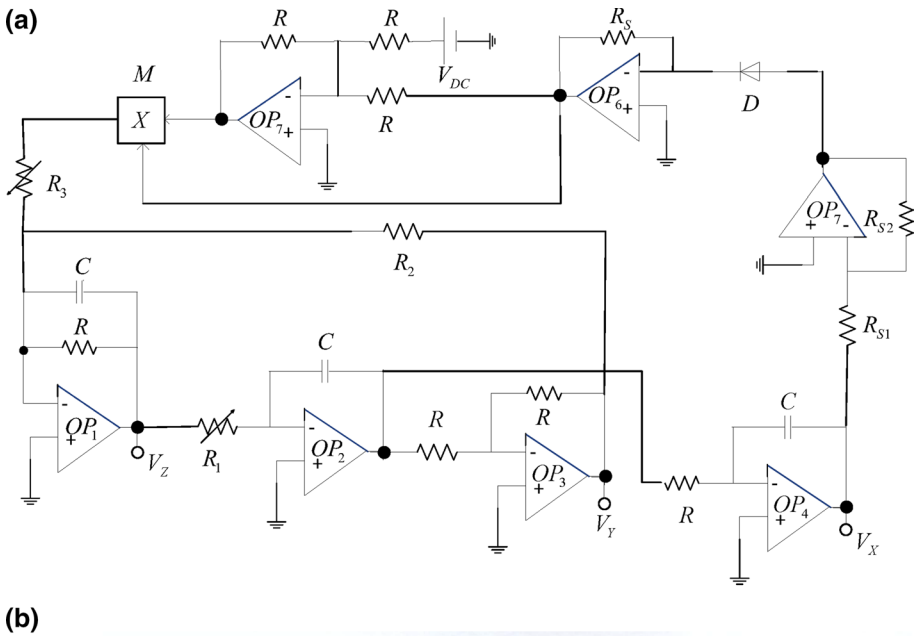

Fig. 9 (Color online) Circuit diagram (**a**) and printed circuit board (**b**) of the proposed jerk oscillator

the diode is given by the relation: $I_d = I_s \left[e^{\left(-\frac{R_{s2}}{R_{s1}} \frac{V_x}{\eta V_t} \right)} - 1 \right]$ where I_s is the reversed satured current, η is an ideal factor and V_t is the thermal temperature of the experimental room. The operations of addition, subtraction and integration are implemented by operational amplifiers OP_4, OP_3 and OP_1 (TL084 integrated circuit) associated with ceramic capacitors and high precision resistors. The resistors R_1 and R_3 are knob resistors. The non-linear term in the proposed autonomous Morse jerk oscillator is successfully implemented by combining a diode and an analogue multiplier device. By applying the Kirchhoff's laws on circuit of Fig. 9, the following nonlinear differential equations are obtained:

$$\frac{dV_x}{dt} = \frac{1}{RC} V_y, \tag{7a}$$

$$\frac{dV_y}{dt} = \frac{1}{R_1 C} V_z, \tag{7b}$$

$$\frac{dV_z}{dt} = -\frac{1}{RC} V_z - \frac{1}{R_2 C} V_y - \frac{1}{R_3 C} \left[1 - R_S I_S \exp\left(-\frac{R_{S2} V_x}{R_{S1} \eta V_T} \right) \right] R_S I_S \exp\left(-\frac{R_{S2} V_x}{R_{S1} \eta V_T} \right), \tag{7c}$$

where V_x, V_y, V_z are the output voltages of the operational amplifiers OP_1, OP_2 and OP_4, respectively. Adopting a time unit of RC=10^{-4} s, the parameters of system (2) are defined in terms of the values of capacitors and resistors as follows:$\delta = 10^{-4}/R_1 C$,$\gamma = 10^{-4}/R_2 C$, $\beta = 10^{-4}/R_3 C$, and $\alpha = 10^{-4}/RC$.We choose convenient values for resistors R=10 kΩ, capacitor $C = 10\,nF$, R_{S2}=0.494 kΩ, R_{S1}= 10 kΩ and $R_S I_S$=1 V to implement the electronic circuit described by system (3). The observations from the oscilloscope of the phase portraits by using the above values of resistors are shown in Fig. 10.
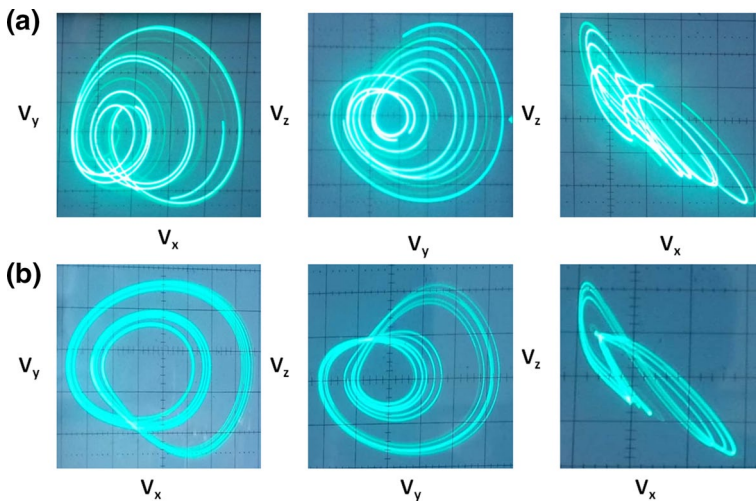

Fig. 10 (Colour online) Phase portraits of chaotic attractors observed on oscilloscope. In panels 1, 2, and 3, we depict the phase portraits in planes (V_x, V_y), (V_y, V_z) and (V_x, V_z), respectively. The values resistances are $R = 10$ kΩ, $R_1 = 0.349$ kΩ, $R_2 = 65.5$ kΩ, $R_3 = 67.5$ kΩ (first line reproduces Fig. 3) and $R = 10$ kΩ, $R_1 = 0.274$ kΩ, $R_2 = 65.5$ kΩ, $R_3 = 67.5$ kΩ (second line reproduces Fig. 6a–c)

The experimental results of Fig. 10 have in a good qualitative agreement with the numerical results of Figs. 3, 6a–c. PSIM software is used to validate the coexistence between periodic oscillations and one scroll-chaotic attractor as shown in Fig. 11 because it is not easy to achieve special initial voltages of three capacitors in hardware circuit experiment [8].

A good qualitative agreement is shown between coexistence attractors illustrated in Fig. 11 using PSIM software and the coexistence attractors obtained during the numerical simulations results of Fig. 7.

4 Controls of the signal amplitudes, chaotic behavior and coexisting attractors in the proposed autonomous Morse jerk oscillator

The goal of this section is to control the signal amplitudes, chaotic behavior and coexisting attractors in the proposed jerk oscillator.
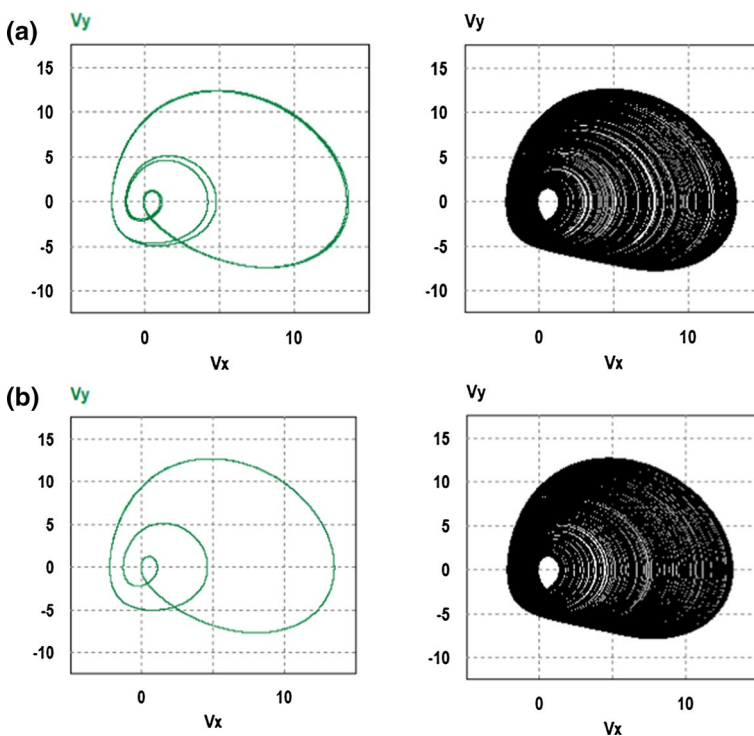

Fig. 11 The phase portraits in plane (V_x, V_y) of coexisting attractors observed on PSIM. The values resistances are: **a** $R = 10\,\text{k}\Omega$, $R_1 = 0.73\,\text{k}\Omega$, $R_2 = 60.024\,\text{k}\Omega$, $R_3 = 23\,\text{k}\Omega$ and **b** $R = 10\,\text{k}\Omega$, $R_1 = 0.78\,\text{k}\Omega$, $R_2 = 60.024\,\text{k}\Omega$, $R_3 = 23\,\text{k}\Omega$. Initial conditions are: **a1** and **b1** $(Vx(0), Vy(0), Vz(0)) = (-2.0V, -4.0V, 0.0V)$, **a2** and **b2** $(Vx(0), Vy(0), Vz(0)) = (2.0V, 2.0V, 2.0V)$

4.1 Partial and total controls of the signal amplitudes

In this subsection, it is demonstrated that system (2) has the feature of partial and total control of the signal amplitudes. The state variable x appears only in the third equation of system (2). So, its amplitude can be controlled by replacing $x \to x + \zeta$ into system (2) where ζ is a boosting controller. Then, system (2) becomes:

$$\dot{x} = y, \tag{8a}$$

$$\dot{y} = \delta z, \tag{8b}$$

$$\dot{z} = -z - \gamma y - \beta\left[1 - e^{-\alpha(x+\zeta)}\right]e^{-\alpha(x+\zeta)}. \tag{8c}$$

System (8) has only one equilibrium point $E_1 = (-\zeta, 0, 0)$. The local stability of $E_1 = (-\zeta, 0, 0)$ reveals that if $\delta > 0$, system (8) has a Hopf bifurcation when β passes through the critical value $\beta_H = \gamma/\alpha$. So, the stability of equilibrium point $E_1 = (-\zeta, 0, 0)$ is independent from the boosting controller ζ. The average values of the state variables x, y and z versus the boosting controller ζ are plotted in Fig. 12 in order to check the amplitude control of the state variable x.

By increasing the boosting controller ζ, the average of the state variable x decreases while other two state variables y and z remain unchanged as shown in Fig. 12. The phase portraits and time series of the state variable x of system (8) are presented in Fig. 13 for different values of boosting controller ζ.

The amplitude of chaotic signal x is boosted from a bipolar signal to unipolar signal by decreasing the boosting controller ζ as shown in Fig. 13.

The feature of total amplitude control in system (2) can be demonstrated by inserting $x \to x/\varepsilon$, $y \to y/\varepsilon$ and $z \to z/\varepsilon$ in system (2) where ε is a control parameter. So, system (3) becomes:

$$\dot{x} = y, \tag{9a}$$

$$\dot{y} = \delta z, \tag{9b}$$

Fig. 12 (Color online) The average values of the state variables x (black), y(blue) and z (red) versus the boosting controller ζ for $\alpha = 1$, $\gamma = 0.16$, $\delta = 18$ and $\beta = 0.6$
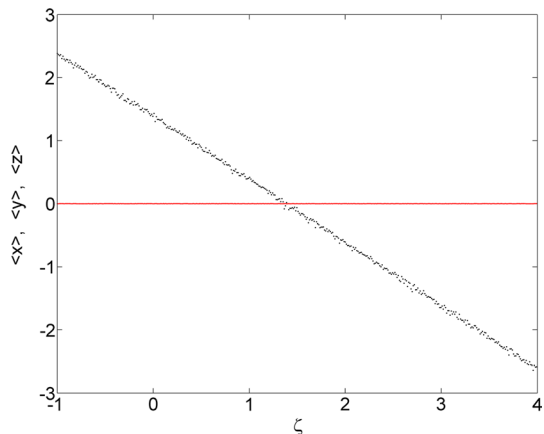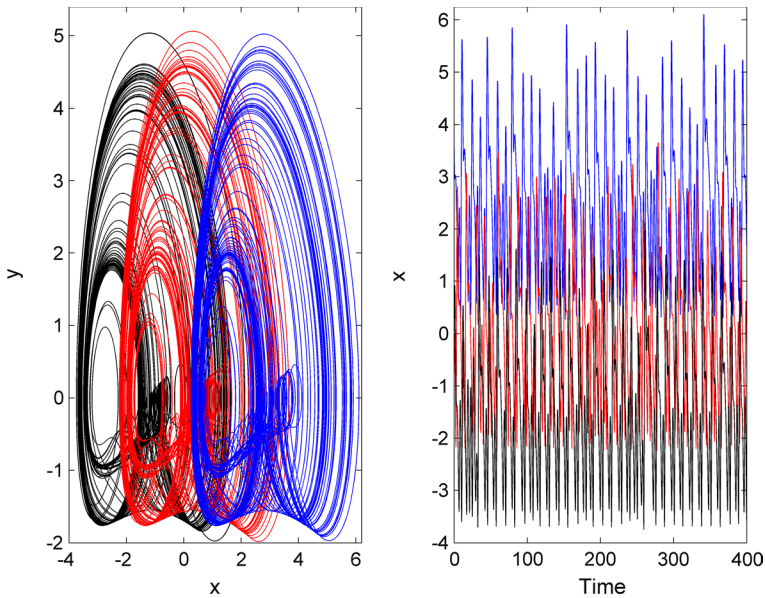
Fig. 13 Phase portraits in the plane (x, y) and time series of the signal x of system (9) for $\alpha = 1$, $\gamma = 0.16$, $\delta = 18, \beta = 0.6$ and different values of boosting controller ζ: $\zeta = 3$(black), $\zeta = 1.5$ (red) and $\zeta = -1$ (blue). Initial conditions are $(x(0), y(0), z(0)) = (0.1, 0.1, 0.1)$

$$\dot{z} = -z - \gamma y - \varepsilon \beta \left[1 - \exp\left(-\alpha x / \varepsilon\right)\right] \exp\left(-\alpha x / \varepsilon\right). \tag{9c}$$

System (9) has only one equilibrium point $O = (0, 0, 0)$. The local stability of $O = (0, 0, 0)$ shows that if $\delta > 0$, system (9) has a Hopf bifurcation when β passes through the critical value $\beta_H = \gamma / \alpha$. So the stability of equilibrium point $O = (0, 0, 0)$ is independent from the control parameters ε. In Fig. 14, the phase portraits of system (9) are depicted for different values of control parameter ε.

The amplitudes of chaotic signals x, y and z are controlled simultaneously by varying the control parameter ε as shown in Fig. 14.

4.2 Chaos control in proposed autonomous chaotic Morse jerk oscillator

The aim of this subsection is to suppress chaotic behavior and stabilize system (2) at its equilibrium $O = (0, 0, 0)$. To achieve this goal, it is introduced an external feedback control law $u = \begin{bmatrix} u_1 & u_2 & u_3 \end{bmatrix}^T$ where for simplicity it is chosen $u_{i \neq 2} = 0$ and $u_2 = -k(y - y_0)$, y_0 being the first coordinate of the equilibrium point O $(x_0 = 0, \ y_0 = 0, \ z_0 = 0)$ and k is the positive feedback control gain. The controlled system takes the form:

$$\frac{dx}{dt} = y, \tag{10a}$$

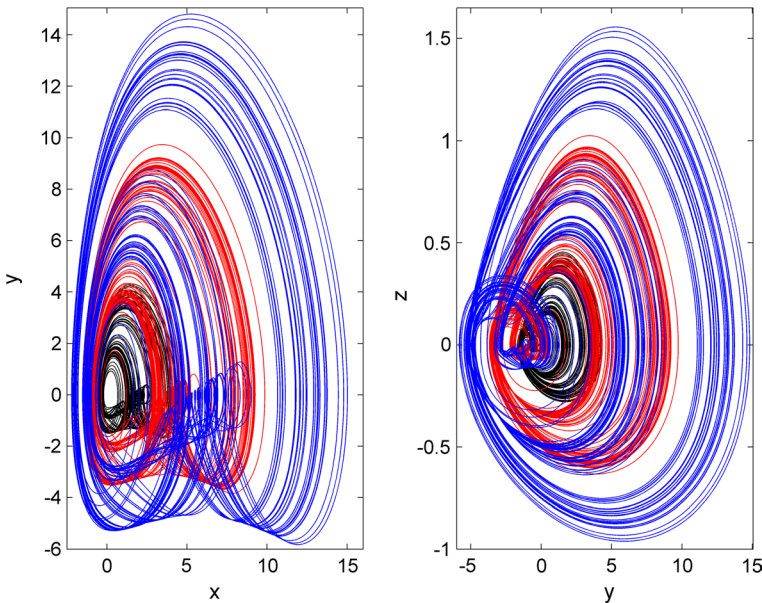$$\frac{dy}{dt} = \delta z - k(y - y_0), \tag{10b}$$

Fig. 14 (Color online) Phase portraits in the planes (x, y) and (y, z) of system (9) for $\alpha = 1$, $\gamma = 0.16$, $\delta = 18, \beta = 0.6$ and different values of control parameter ε: $\varepsilon = 0.85$(black), $\varepsilon = 2$ (red) and $\varepsilon = 3$ (blue). Initial conditions are$(x\,(0),\, y\,(0),\, z\,(0)) = (0.1,\, 0.1,\, 0.1)$

$$\frac{dz}{dt} = -z - \gamma y - \beta\left[1 - \exp\left(-\alpha x\right)\right]\exp\left(-\alpha x\right). \tag{10c}$$

The controlled system (10) has only one equilibrium point $O = (0, 0, 0)$ and its Jacobian matrix has the characteristic polynomial:

$$\lambda^3 + (k + 1)\lambda^2 + (k + \delta\gamma)\lambda + \alpha\beta\delta = 0. \tag{11}$$

The Routh–Hurwitz conditions for the stability of the controlled system (10) at its equilibrium are the following:

$$k + 1 > 0, \tag{12a}$$

$$\alpha\beta\delta > 0, \tag{12b}$$

$$k^2 + (1 + \gamma\delta)k + \delta(\gamma - \alpha\beta) > 0. \tag{12c}$$

For $\alpha = 1$, $\gamma = 0.16$, $\beta = 0.6$ and $\delta = 18$, the inequalities (12c) is positive for $k < -5.36$ and $k > 1.48$. According to the set of inequalities (12), the equilibrium point $O = (0, 0, 0)$ is stable for $k > 1.48$ and unstable for $k < 1.48$. Using the numerical simulations of system (10) for $\alpha = 1$, $\gamma = 0.16$, $\beta = 0.6$ and $\delta = 18$, the bifurcation diagram of $x(t)$ and the LLE versus the control gain k is plotted in Fig. 15 in order to check the validity of the analytical results found.

From Fig. 15a, a reverse period-doubling to chaos interspersed with periodic windows is observed up to $k \approx 1.48$ where a Hopf bifurcation appears followed by no oscillation
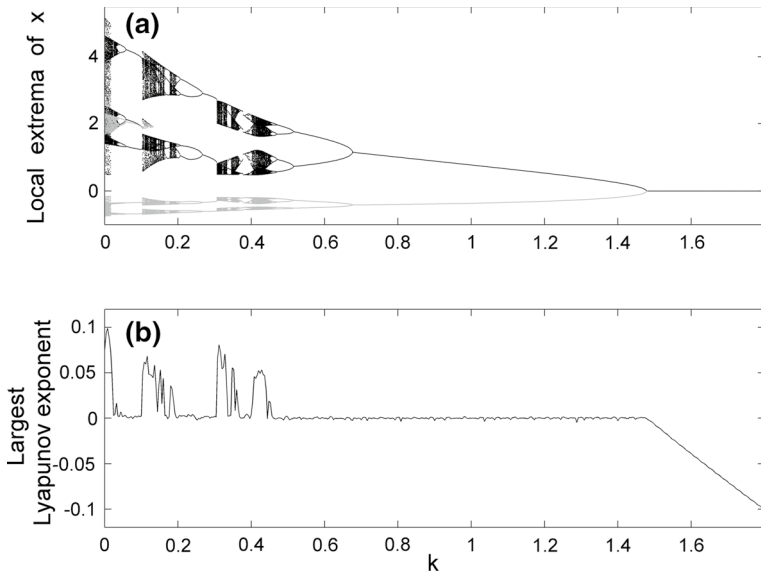
Fig. 15 Bifurcation diagram depicting the local maxima (black dots) and local minima (gray dots) of $x(t)$ (a) and the LLE (b) versus the control gain k for $\alpha = 1$, $\gamma = 0.16$, $\beta = 0.6$ and $\delta = 18$
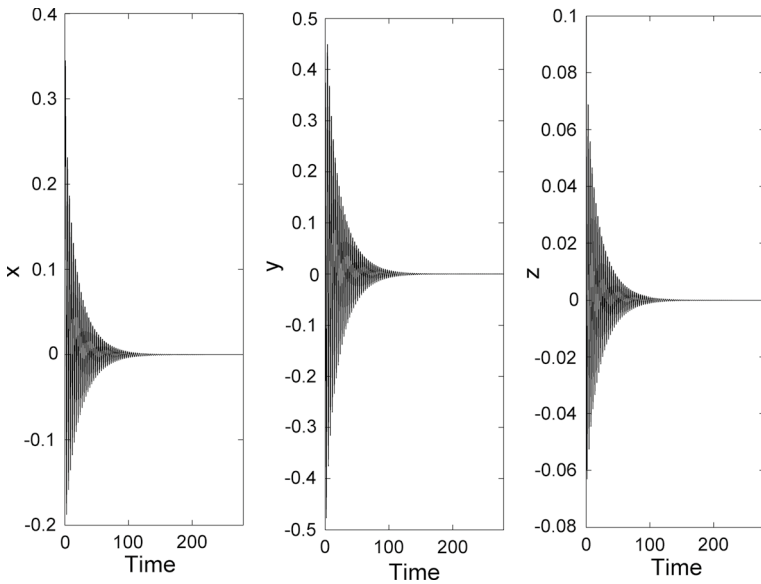

Fig. 16 Time series of the outputs of x, y and z for $k = 1.6$, $\alpha = 1$, $\gamma = 0.16$, $\beta = 0.6$ and $\delta = 18$. The initial condition is $(x(0), y(0), z(0)) = (0.1, 0.1, 0.1)$

(equilibrium point). Therefore, the analytical results confirm the results obtained during numerical integration of controlled system (10) as shown in Fig. 15. The dynamical behaviors found in Fig. 15a are confirmed by the LLE shown in Fig. 15b. For $k = 1.6$, the time series of the outputs of x, y and z is plotted in Fig. 16.

The trajectories of controlled system (10) are controlled to the equilibrium point $O = (0, 0, 0)$ as shown in Fig. 16.

4.3 Control of coexisting attractors in proposed autonomous Morse jerk oscillator

In the most dynamical systems, multistability can create inconveniences which contribute to reduce considerably the performances of such systems. Several methods have been proposed and developed for the control of multistabilty in multistable oscillators [2, 20, 38, 40, 41]. It is demonstrated that such methods are capable to stabilize the dynamics of these systems to a monostable state [38, 40, 41]. Among these methods, linear augmentation method is one of the most used methods because of its large applicability, simplicity in designing and physical implementation. In order to destroy the coexistence between periodic and chaotic attractors, system (2) is coupled with a linear system as follows:

$$\dot{x} = y, \tag{13a}$$

$$\dot{y} = \delta z, \tag{13b}$$

$$\dot{z} = -z - \gamma y - \beta \left[1 - \exp\left(-\alpha x\right)\right] \exp\left(-\alpha x\right) + \mu \mathrm{w}, \tag{13c}$$

$$\dot{\mathrm{w}} = -\eta \mathrm{w} - \mu(z - \theta), \tag{13d}$$

where μ is the coupling strength, θ is the control parameter which serves to locate the position of equilibrium point and η is the decay parameter of the linear system w. System (13) has no-equilibrium point for $4\theta\mu^2/\eta\beta > 1$ while for $4\theta\mu^2/\eta\beta < 1$ two equilibrium points $E_1 = (-x_1/\alpha, 0, 0, \theta\mu/\eta)$ and $E_2 = (-x_2/\alpha, 0, 0, \theta\mu/\eta)$ where $x_{1,2} = \ln\left(1/2 \pm \sqrt{1 - 4\theta\mu^2/\eta\beta}\middle/2\right)$. The bifurcation diagram depicting local extrema of the controlled system (13) and the corresponding LLE versus the coupling strength μ are shown in Fig. 17.

By increasing the coupling strength μ, the bifurcation diagram of the controlled system (13) in Fig. 17a displays a reverse period-doubling bifurcation to chaotic behavior interspersed with periodic windows. By further increasing the coupling strength μ, a limit cycle is observed up to $\mu \approx 0.3156$ where a Hopf bifurcation occurs followed by converging of the trajectories of the controlled system (13) to the equilibrium point E_2. The dynamical behaviors found in Fig. 17a are confirmed by the LLE shown in Fig. 17b. Therefore, the controlled system (13) transforms the multistable attractors to desired monostable attractors.

5 Conclusion

In this paper, an autonomous Morse jerk oscillator was proposed and analyzed. It was demonstrated that the proposed jerk oscillator displays Hopf bifurcation, antimonotonicity, one scroll-chaotic attractor, periodic and chaotic bubbles and coexistence between
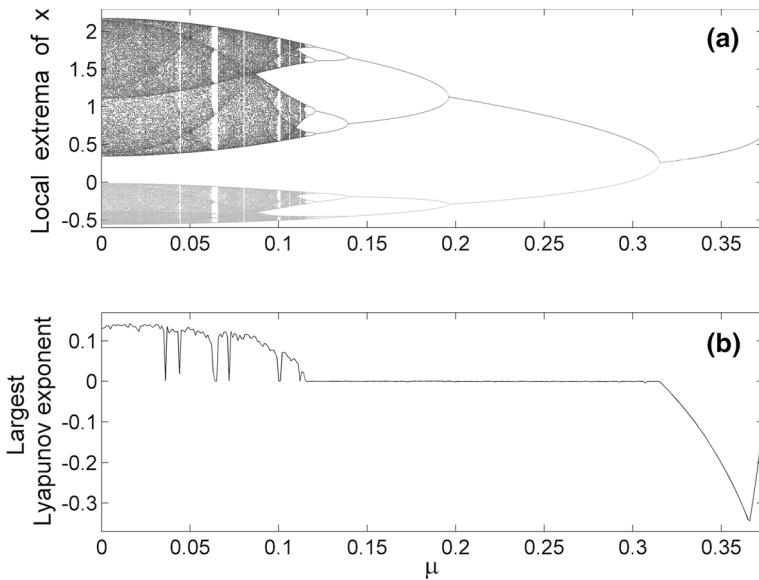
Fig. 17 Bifurcation diagrams depicting the maxima (black shaded areas) and minima (grey shaded areas) of $x(t)$ **a** and **b** the corresponding LLE versus the coupling strength μ for $\eta = 0.7$, $\theta = 0.5$, $\alpha = 1$, $\gamma = 0.16$, $\beta = 0.6$ and $\delta = 25$

periodic and one scroll-chaotic attractors by tuning the parameters. Then, an analogue circuit was designed to realize the rate-equations describing the proposed autonomous Morse jerk oscillator. The experimental/PSIM results were shown consistency with numerical simulations results. Then, a flexible chaotic autonomous jerk oscillator with partial and total amplitude controls was achieved by adding two new parameters in the rate-equations describing the proposed Morse jerk oscillator. Moreover, a single linear feedback controller was used to stabilize the chaotic proposed jerk oscillator to its unique equilibrium point. Finally, the coexisting of attractors found in the proposed jerk oscillator was controlled to a desired trajectory by using a linear augmentation method.

References

[1] Abirami, K., Rajasekar, S., Sanjuan, M.A.F.: Vibrational resonance in the Morse oscillator. Pramana **81**(1), 127–141 (2013)

[2] Ainamon, C., Kingni, S.T., Tamba, V.K., et al.: Dynamics, circuitry implementation and control of an autonomous Helmholtz Jerk oscillator. J. Control Autom. Electr. Syst. **30**, 501–511 (2019)

[3] Akgul, A., Arslan, C., Aricioglu, B.: Design of an interface for random number generators based on integer and fractional order chaotic systems. Chaos Theory Appl. **1**, 1–18 (2019)

[4] Awrejcewicz, J., Kudra, G., Wasilewski, G.: Chaotic zones in triple pendulum dynamics observed experimentally and numerically. In: Applied Mechanics and Materials. Trans Tech Publ. (2008)

[5] Bakemeier, L., Alvermann, A., Fehske, H.: Route to chaos in optomechanics. Phys. Rev. Lett. **114**(1), 013601 (2015)

[6] Bao, B.-C., et al.: Extreme multistability in a memristive circuit. Electron. Lett. **52**(12), 1008–1010 (2016)

[7] Bao, B., et al.: Coexisting infinitely many attractors in active band-pass filter-based memristive circuit. Nonlinear Dyn. **86**(3), 1711–1723 (2016)

[8] Bao, B., et al.: Hidden extreme multistability in memristive hyperchaotic system. Chaos, Solitons Fractals **94**, 102–111 (2017)

[9] BenÍtez, S., Acho, L., Guerra, R.J.: Chaotification of the Van der Pol system using Jerk architecture. IEICE Trans. Fundam. Electron. Commun. Comput. Sci. **89**(4), 1088–1091 (2006)

[10] Bier, M., Bountis, T.C.: Remerging Feigenbaum trees in dynamical systems. Phys. Lett. A **104**(5), 239–244 (1984)

[11] Blażejczyk-Okolewska, B., Kapitaniak, T.: Co-existing attractors of impact oscillator. Chaos, Solitons Fractals **9**(8), 1439–1443 (1998)

[12] Callan, K.E., et al.: Broadband chaos generated by an optoelectronic oscillator. Phys. Rev. Lett. **104**(11), 113901 (2010)

[13] Caponetto, R., et al. A new chaotic system for the authentication and electronic certification procedures. In: Electronics, Circuits and Systems, 1999. Proceedings of ICECS'99. The 6th IEEE International Conference on. 1999. IEEE.

[14] Carlen, E., et al.: Kinetic hierarchy and propagation of chaos in biological swarm models. Physica D **260**, 90–111 (2013)

[15] Chudzik, A., et al.: Multistability and rare attractors in van der Pol-Duffing oscillator. Int. J. Bifurc. Chaos **21**(07), 1907–1912 (2011)

[16] Dawson, S.P., et al.: Antimonotonicity: inevitable reversals of period-doubling cascades. Phys. Lett. A **162**(3), 249–254 (1992)

[17] Ding, Y., Zhang, Q.: Impulsive homoclinic chaos in Van der Pol Jerk system. Trans. Tianjin Univ. **16**(6), 457–460 (2010)

[18] Hilborn, R.C.: Chaos and nonlinear dynamics: an introduction for scientists and engineers. Oxford University Press, Oxford (2000)

[19] Hommes, C.H., Nusse, H.E., Simonovits, A.: Cycles and chaos in a socialist economy. J. Econ. Dyn. Control **19**(1–2), 155–179 (1995)

[20] Kamdoum Tamba, V., Fotsin, H.B.: Multistability and its control in a simple chaotic circuit with a pair of light-emitting diodes. Cybern. Phys. **6**, 114–120 (2017)

[21] Kapitaniak, T., Leonov, G.A.: Multistability: uncovering hidden attractors. Euro. Phys. J. Spl. Top. **224**(8), 1405–1408 (2015)

[22] Kingni, S.T., et al.: Theoretical analysis of semiconductor ring lasers with short and long time-delayed optoelectronic and incoherent feedback. Opt. Commun. **341**, 147–154 (2015)

[23] Krempl, S., et al.: Optimal stimulation of a conservative nonlinear oscillator: Classical and quantum-mechanical calculations. Phys. Rev. Lett. **69**(3), 430 (1992)

[24] Lai, Q., et al.: Various types of coexisting attractors in a new 4D autonomous chaotic system. Int. J. Bifurc. Chaos **27**(09), 1750142 (2017)

[25] Lai, Q., Chen, S.: Coexisting attractors generated from a new 4D smooth chaotic system. Int. J. Control Autom. Syst. **14**(4), 1124–1131 (2016)

[26] Lai, Q., Wang, L.: Chaos, bifurcation, coexisting attractors and circuit design of a three-dimensional continuous autonomous system. Optik Int. J. Light Electron Opt. **127**(13), 5400–5406 (2016)

[27] Leonhardt, U.: State reconstruction of anharmonic molecular vibrations: Morse-oscillator model. Phys. Rev. A **55**(4), 3164 (1997)

[28] Li, C., Sprott, J.C.: An infinite 3-D quasiperiodic lattice of chaotic attractors. Phys. Lett. A **382**(8), 581–587 (2018)

[29] Li, C., Sprott, J.C., Mei, Y.: An infinite 2-D lattice of strange attractors. Nonlinear Dyn. **89**(4), 2629–2639 (2017)

[30] Louodop, P., et al.: Practical finite-time synchronization of jerk systems: Theory and experiment. Nonlinear Dyn. **78**(1), 597–607 (2014)

[31] Muthuswamy, B., Chua, L.O.: Simplest chaotic circuit. Int. J. Bifurc. Chaos **20**(05), 1567–1580 (2010)

[32] Nana, B., Woafo, P., Domngang, S.: Chaotic synchronization with experimental application to secure communications. Commun. Nonlinear Sci. Numer. Simul. **14**(5), 2266–2276 (2009)

[33] Ott, E.: Chaos in dynamical systems. Cambridge University Press, Cambridge (2002)

[34] Pettitt, B.: The Morse oscillator and second-order perturbation theory. J. Chem. Educ. **75**(9), 1170 (1998)

[35] Pham, V.-T., et al.: Simple memristive time-delay chaotic systems. Int. J. Bifurc. Chaos **23**(04), 1350073 (2013)

[36] Pham, V.-T., et al.: Nonlinear Dynamical Systems with Self-Excited and Hidden Attractors, vol. 133. Springer (2018)

[37] Piper, J.R., Sprott, J.C.: Simple autonomous chaotic circuits. IEEE Trans. Circuits Syst. II: Exp. Br. **57**(9), 730–734 (2010)

[38] Pisarchik, A.N., Feudel, U.: Control of multistability. Phys. Rep. **540**, 167–218 (2014)

[39] Rial, J.A.: Abrupt climate change: chaos and order at orbital and millennial scales. Glob. Planet. Change **41**(2), 95–109 (2004)

[40] Sharma, P.R., Shrimali, M.D., Prasad, A., Feudel, U.: Controlling bistability by linear augmentation. Phys. Lett. A **377**, 2329–2332 (2013)

[41] Sharma, P.R., Shrimali, M.D., Prasad, A., Kuznetsov, N.V., Leonov, G.A.: Control of multistability in hidden attractors. Eur. Phys. J. Special Topics **224**, 1485–1491 (2015)

[42] Sprott, J.C.: Simple chaotic systems and circuits. Am. J. Phys. **68**(8), 758–763 (2000)

[43] Sprott, J.C.: Elegant chaos: algebraically simple chaotic flows. World Scientific, Singapore (2010)

[44] Sprott, J.C., et al.: Megastability: Coexistence of a countable infinity of nested attractors in a periodically-forced oscillator with spatially-periodic damping. Euro. Phys. J. Spl. Top **226**(9), 1979–1985 (2017)

[45] Takougang Kingni, S., Hervé Talla Mbé, J., Woafo, P.: Semiconductor lasers driven by self-sustained chaotic electronic oscillators and applications to optical chaos cryptography. Chaos: Interdiscip. J. Nonlinear Sci. **22**(3), 033108 (2012)

[46] Tamba, V.K., et al.: Coexistence of attractors in autonomous Van der Pol-Duffing jerk oscillator: Analysis, chaos control and synchronisation in its fractional-order form. Pramana **91**(1), 12 (2018)

[47] Tamba, V.K., et al.: An Autonomous Helmholtz Like-Jerk Oscillator: Analysis, Electronic Circuit Realization and Synchronization Issues. In: Nonlinear Dynamical Systems with Self-Excited and Hidden Attractors, pp. 203–227. Springer (2018)

[48] Tang, Y.X., Khalaf, A.J., Rajagopal, K., Pham, V.T., Jafari, S., Tian, Y.: A new nonlinear oscillator with infinite number of coexisting hidden and self-excited attractors. Chin. Phys. B **27**(4), 40502–040502 (2018)

[49] Wu, J., Cao, J.: Linear and nonlinear response functions of the Morse oscillator: Classical divergence and the uncertainty principle. J. Chem. Phys. **115**(12), 5381–5391 (2001)

[50] Zuppa, L.A., Garrido, J.C.R., Escobar, S.B.: A chaotic oscillator using the Van der Pol dynamic immersed into a Jerk system. WSEAS Trans. Circuits Syst. **3**(1), 198–199 (2004)